Magazine of Civil Engineering

ISSN 2712-8172

journal homepage: http://engstroy.spbstu.ru/

Research article

UDC 69

DOI: 10.34910/MCE.129.10

Buckling of a viscoelastic anisotropic fiber reinforced plate under rapidly increasing shear load

B.Kh. Eshmatov[1], ***M.M. Mirsaidov***[1], ***R.A. Abdikarimov***[2], ***N.I. Vatin***[3] ✉

[1] *Tashkent Institute of Irrigation and Agricultural Mechanization Engineers (TIIAME), Tashkent, Uzbekistan*

[2] *Tashkent Institute of Architecture and Civil Engineering, Tashkent, Uzbekistan*

[3] *Peter the Great St. Petersburg Polytechnic University, St. Petersburg, Russian Federation*

✉ *vatin@mail.ru*

Keywords: dynamic stability, viscoelastic anisotropic fiber reinforced plate, system of integro-differential equations, weakly-singular Koltunov–Rzhanitsyn kernel, critical time

Abstract. The problem of stability of a viscoelastic anisotropic fiber reinforced plate under the action of a rapidly increasing (dynamic) shear load in a geometrically nonlinear formulation is considered. The mathematical model of the problem is described by a system of nonlinear partial integro-differential equations with singular relaxation kernels. The Bubnov–Galerkin method is used to obtain systems of ordinary nonlinear integro-differential equations. The solution of the system of resolving equations is carried out by a numerical method based on quadrature formulas. To substantiate the accuracy and adequacy of the obtained results, a test problem is solved. A stability criterion for reinforced plates under the action of shear loads is introduced. Depending on various geometric, physical, and mechanical characteristics of the material, the behavior of the reinforced plate is investigated. In particular, it is shown that taking into account the viscoelastic properties of the material leads to a decrease in the critical time, and therefore in the critical force. Depending on various geometric and physical parameters, the difference in critical time values for elastic and viscoelastic plates in some cases is more than 15 %. It is also shown that an increase in the angle of fiber direction in the plates leads to a decrease in the critical time. Among the single-layer reinforced plates, the plate with a fiber direction of 0° is the most resistant to shear loads. An increase in the number of layers in a reinforced plate while maintaining its thickness does not always favorably affect the stability of the plate. In the case of three-layer viscoelastic plates made from KAST-V material with fibers oriented in the direction of 45°/–45°/45°, they are less stable than double-layer plates but more stable than single-layer ones while maintaining equal thicknesses of all three structures.

Funding: This research was financially supported by the Ministry of Science and Higher Education of the Russian Federation, project FSEG-2022-0010 (agreements No. 075-03-2022-010 dated 14.01.2022 and No. 075-01568-23-04 dated 28.03.2023; additional agreements No. 075-03-2022-010/10 dated 09.11.2022 and No. 075-03-2023-004/4 dated 22.05.2023).

Citation: Eshmatov, B.Kh., Mirsaidov, M.M., Abdikarimov, R.A., Vatin, N.I. Buckling of a viscoelastic anisotropic fiber reinforced plate under rapidly increasing shear load. Magazine of Civil Engineering. 2024. 17(5). Article no. 12910. DOI: 10.34910/MCE.129.10

1. Introduction

The use of composite materials, which exhibit a unique combination of mechanical and operational characteristics, has become indispensable in industry. By ingeniously combining different substances, compositions, and component ratios, these materials yield products with optimal characteristics of their raw

ingredients. Composite materials offer such essential qualities as elasticity, strength, heat resistance, electrical conductivity, etc.

The effectiveness of using composite materials in various structures largely depends on the refinement of mathematical models and calculation methods. Developing calculation methods for structural elements composed of composite materials requires a mathematical problem formulation that reflects the distinctive deformation characteristics of the material, which can substantially impact their load-bearing capacity.

Currently, the volume of scientific research dedicated to the study of structures from composite materials, encompassing various physical and geometric parameters, has a steady upward trend.

A comprehensive review of existing literature on analyzing oscillatory phenomena in fiber reinforced composites is available in [1].

The laminated composite plate dynamic responds, when a mass hits it in the center, and energy transfers from the mass to the plate, were studied in [2]. The plate had initial stress before the impact load. The nonlinear integral equation was used. The key finding was that the higher the initial tension in the plate, the stronger the impact force would be. Additionally, a higher initial tension reduces the amount of energy transferred from the mass to the plate.

The free oscillations and dynamic behavior of polymer composites reinforced with surface-modified basalt fiber were investigated in [3]. Natural frequencies and damping coefficients of layered composites were examined through impact testing and dynamic mechanical analysis.

Meanwhile, [4] studied the effect of stacking and hybridization sequences on the damping properties of epoxy composites made of flax-carbon twill. The dynamic characteristics are examined using the pulse method. For modeling damping, the finite element method is implemented to evaluate the energy dissipation in each layer of carbon-linen laminates.

The paper [5] deals with the free vibration modal analysis of hybrid laminates using a finite element model based on the third order shear deformation theory and the first-order shear deformation theory. A computer code has been developed using MATLAB, 2013. The experimental investigation of the free vibration of hybrid laminates made of carbon and glass fibers is conducted. Numerical results are compared with experimental outcomes, contributing to a holistic understanding.

Further investigations explore the stability of structures made of composite materials. The work [6] investigates the potential for using the produced green composite in load-bearing structures and scrutinize bending properties under axial compression using numerical analysis and ANSYS software.

Additionally, the work [7] examines the stability loss of layered composites when the influence of orthotropic materials is taken into account. This influence justifies the importance of considering orthotropic properties in analyzing the dynamic process.

However, relatively less attention has been dedicated to studying dynamic stability in structures made of composite materials under the influence of shear loads. Most composite materials have pronounced viscoelastic properties. Practical experience in addressing various mechanical problems underscores the significance of incorporating the viscoelastic properties of structural materials. In this regard, the Boltzmann–Volterra integral models are good models that integrate both the relaxation and creep processes.

The developed numerical method based on quadrature formulas was explained in detail in [8]. It facilitates the solution of systems of linear and nonlinear integro-differential equations with different kernels. This method, characterized by its simplicity, convenience, and efficiency in terms of computational time, delivers highly accurate results and accommodates various dynamic viscoelasticity problems. Notably, [9–11] present a series of practical problems solved using the developed method, with the numerical results closely aligned with experimental findings.

The study [12] presents a non-linear dynamic analysis of a cross-ply laminated composite with fiber spacing plates under in-plane loading. The first order shear deformation theory and von Karman nonlinearity are used. Eight-node isoperimetric quadrilateral elements with five degrees of freedom per node are used to maintain geometric nonlinearity. The investigation explores a variety of fiber spacings and orientations to understand their influence on the behavior of samples under this loading condition. The dynamic equilibrium equations are solved using the Newmark integration technique. The nonlinear dynamic analysis examines the effects of changing fiber spacing with various changes in volume percentage and diverse fiber orientations. These variations were found to significantly influence the nonlinear dynamic behavior of the laminated composite plates.

The study [13] investigates the nonlinear bending behavior of laminated composite plates under static and dynamic loads. The plate was reinforced by single-walled carbon nanotubes' fibers and nanoclay particles. The Halpin–Tsai mathematical model, which is based on the self-consistent field method, is applied. This model can be used to predict the modulus of composite materials. The computer program is created to solve this model. The program also considers different support conditions for the plate (clamped or simply supported).

The research [14] investigates how adding fillers can improve the strength and vibration response of laminated composite plates. The laminated composite plates are fabricated by open layup process with epoxy resin, E-glass fiber reinforcement, and fly ash and graphene fillers (up to 5 % total volume). The total fiber and filler content is limited to 60 % by weight. The laminated composite plates are designed with various fly ash-to-graphene ratios. A custom-built vibration testing system is used to measure the free and forced vibrations of simply supported laminated composite plates. These experimental results are compared to mathematical models based on fifth order shear deformation theory and finite element analysis. Finally, the effect of circular holes on the laminated composite plates' vibration characteristics is investigated using simulations. These simulations analyze how hole size and location impact the modal frequencies of the laminated composite plates.

The research [15] investigates the vibration of a curved beam made from layers of composite material reinforced with graphene platelets. The amount of reinforcement varies between layers, creating a specific type of material. The study analyses both vibrations caused by the beam itself (free vibration) and vibrations caused by a moving load (forced vibration). The analysis is validated using existing data and then expanded to explore how different factors influence the vibration. The findings show that the shape of the beam, the amount of graphene reinforcement, and its distribution affect the vibration intensity of the beam in both scenarios. Simply put, a stiffer beam with more graphene reinforcement vibrates less.

The research [16] studies how laminated beams made of composite materials vibrate when they have a separation layer running across their width. The study considers both in-plane and out-of-plane vibrations. The researchers use a computer simulation technique and a special method to account for contact between the separated layers. This research investigates the natural frequencies of a damaged beam and its response to various forces. The analysis includes both constant and moving force applications. The results of the present study are verified by comparing them with those available in the literature. This work provides a complete picture of how these damaged beams vibrate in all directions.

The research [17] focuses on the vibration characteristics of rectangular composite panels used in structures like automobiles. These panels are designed to replace heavier metals for improved efficiency. The study examines how different fiber orientations within the composite panels affect their vibration under external forces. Two methods, analytical and numerical, are used to analyze the vibration behavior. The findings show that the way the fibers are oriented significantly impacts vibration, and this knowledge can be used to design composite structures with better vibration control.

The research [18] focuses on fiber-reinforced polymer composites used in car parts like inlet/exhaust flange gaskets. These composites are desirable due to their strength-to-weight ratio and other properties. However, machining processes like drilling can cause delamination, which can grow and lead to sudden part failure. This study aims to identify such damage beforehand. The research method involves vibration analysis (modal and harmonic) using finite element analysis software. The analysis is performed on a model of a gasket, initially intact and then with deliberate delamination at the drilling location. Different delamination locations and materials are simulated. The results for intact and delaminated plates are compared, including vibration modes, resonance frequencies, and stress distribution.

The study [19] investigates how delamination, a layering separation common in fiber reinforced polymer composites, impacts the vibration and stress behavior of plates with circular holes. It employs a combined approach: the layerwise theory for numerical analysis and the finite element method to simulate delamination effects. The research reveals a significant influence of delamination size on the plate's natural frequency, stress concentration points, and overall impedance.

The research [20] investigates the vibration of composite conical panels made with layers containing different amounts of graphene platelets. The effect of both uniform and non-uniform porosity is also considered. The material properties are estimated using established methods. The analysis uses a specific theory of shells and kinematics to define the energy components. A general method is applied to discretize the energy terms, allowing for various boundary conditions. Standard methods are used to find natural frequencies and track the deflection over time. The results are compared with the available data in the open literature, and new results are presented. The study concludes that both the type of porosity and the graphene platelets distribution significantly affect the frequencies and deflection of the panel.

Despite the abundance of scientific results on structures made of composite materials encompassing diverse physical and geometric parameters, a number of questions remain unanswered. For the first time,

this paper aimed to study the stability of a viscoelastic anisotropic reinforced plate clamped on boundaries constructed from composite material under the influence of rapid, dynamic shear loads.

2. Materials and Methods

The rectangular rigidly pinched fiberglass plate subjected to the dynamic action of shear forces evenly distributed along its edges was considered (Fig. 1). It was assumed that the shear forces increased in proportion to time according to the law

$$P(t) = P_0 \cdot t, \tag{1}$$

where P_0 is the loading rate.

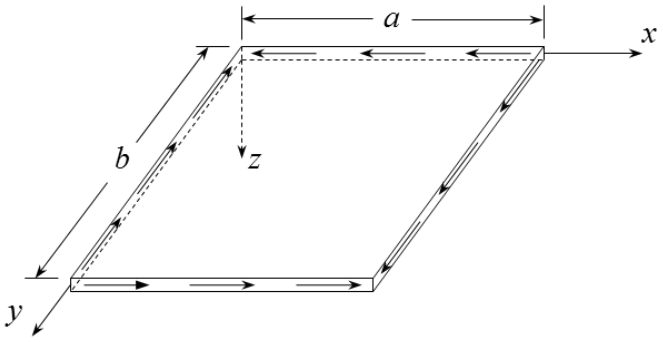

Figure 1. Rectangular plate under shear load.

The classical Kirchhoff–Love theory was employed to develop a mathematical model for a problem. The resulting stresses and moments were determined in the same manner as described in [21, 22]:

$$\begin{aligned}
N_x &= A_{11}^*\varepsilon_x + A_{12}^*\varepsilon_y + A_{16}^*\gamma_{xy} + B_{11}^*\chi_x + B_{12}^*\chi_y + B_{16}^*\chi_{xy},\\
N_y &= A_{12}^*\varepsilon_x + A_{22}^*\varepsilon_y + A_{26}^*\gamma_{xy} + B_{12}^*\chi_x + B_{22}^*\chi_y + B_{26}^*\chi_{xy},\\
N_{xy} &= A_{16}^*\varepsilon_x + A_{26}^*\varepsilon_y + A_{66}^*\gamma_{xy} + B_{16}^*\chi_x + B_{26}^*\chi_y + B_{66}^*\chi_{xy},\\
M_x &= B_{11}^*\varepsilon_x + B_{12}^*\varepsilon_y + B_{16}^*\gamma_{xy} + D_{11}^*\chi_x + D_{12}^*\chi_y + D_{16}^*\chi_{xy},\\
M_y &= B_{12}^*\varepsilon_x + B_{22}^*\varepsilon_y + B_{26}^*\gamma_{xy} + D_{12}^*\chi_x + D_{22}^*\chi_y + D_{26}^*\chi_{xy},\\
M_{xy} &= B_{16}^*\varepsilon_x + B_{26}^*\varepsilon_y + B_{66}^*\gamma_{xy} + D_{16}^*\chi_x + D_{26}^*\chi_y + D_{66}^*\chi_{xy},
\end{aligned} \tag{2}$$

where $A_{ij}^*, B_{ij}^*, D_{ij}^*, i, j = 1,2,6$ are operators of the following form:

$$A_{ij}^*\varphi = \sum_{k=1}^{K}\left(\overline{Q}_{ij}^*\varphi\right)_k\left(z_k - z_{k-1}\right), \quad B_{ij}^*\varphi = \frac{1}{2}\sum_{k=1}^{K}\left(\overline{Q}_{ij}^*\varphi\right)_k\left(z_k^2 - z_{k-1}^2\right),$$

$$D_{ij}^*\varphi = \frac{1}{3}\sum_{k=1}^{K}\left(\overline{Q}_{ij}^*\varphi\right)_k\left(z_k^3 - z_{k-1}^3\right),$$

$$\overline{Q}_{11}^*\varphi = \left[Q_{11}\cos^4\theta + \frac{1}{2}\left(Q_{12} + 2Q_{66}\right)\sin^2 2\theta + Q_{22}\sin^4\theta\right]\left(1 - \Gamma^*\right)\varphi,$$

$$\overline{Q}_{12}^*\varphi = \left[\frac{1}{4}\left(Q_{11} + Q_{22} - 4Q_{66}\right)\sin^2 2\theta + Q_{12}\left(1 - \frac{1}{2}\sin^2 2\theta\right)\right]\left(1 - \Gamma^*\right)\varphi,$$

$$\overline{Q}_{16}^*\varphi = \left[Q_{11}\sin\theta\cos^3\theta - \frac{1}{4}\left(Q_{12} + 2Q_{66}\right)\sin 4\theta - Q_{22}\sin^3\theta\cos\theta\right]\left(1 - \Gamma^*\right)\varphi,$$

$$\bar{Q}_{22}^{*}\varphi=\left[Q_{11}\sin^4\theta+\frac{1}{2}\left(Q_{12}+2Q_{66}\right)\sin^2 2\theta+Q_{22}\cos^4\theta\right]\left(1-\Gamma^{*}\right)\varphi,$$

$$\bar{Q}_{26}^{*}\varphi=\left[Q_{11}\sin^3\theta\cos\theta-\frac{1}{4}\left(Q_{12}+2Q_{66}\right)\sin 4\theta-Q_{22}\sin\theta\cos^3\theta\right]\left(1-\Gamma^{*}\right)\varphi,$$

$$\bar{Q}_{66}^{*}\varphi=\left[\frac{1}{4}\left(Q_{11}-2Q_{12}+Q_{22}\right)\sin^2 2\theta+Q_{66}\cos^2 2\theta\right]\left(1-\Gamma^{*}\right)\varphi,$$

$$Q_{11}=\frac{E_1}{1-\mu_{12}\mu_{21}},\ Q_{22}=\frac{E_2}{1-\mu_{12}\mu_{21}},\ Q_{12}=\frac{E_1\mu_{21}}{1-\mu_{12}\mu_{21}}=\frac{E_2\mu_{12}}{1-\mu_{12}\mu_{21}},\ Q_{66}=G_{12},$$

$$\Gamma^{*}\varphi=\int_0^t\Gamma\left(t-\tau\right)\varphi\left(\tau\right)d\tau$$

Here K is the number of plate layers; E_1, E_2 are the elastic moduli; G_{12} is the shear modulus; μ_{12}, μ_{21} are the Poisson ratios; θ is the angle characterizing the direction of the reinforced fibers relative to the OX axis; Γ^{*} is the integral operator with the relaxation kernel $\Gamma\left(t\right)$.

If the dynamic process is analyzed without considering the propagation of elastic waves, then it becomes possible to discard the inertial terms in the first two equations of the system (3). The relations between the strains in the median surface ε_x, ε_y, γ_{xy}, χ_x, χ_y, χ_{xy} and displacements u, v, w in the x, y, z directions takes into account geometric nonlinearity. In this case, the solution of the resulting system was searched in the form described in the articles [21–23]:

$$\begin{gathered}\varepsilon_x=\frac{\partial u}{\partial x}+\frac{1}{2}\left(\frac{\partial w}{\partial x}\right)^2,\ \varepsilon_y=\frac{\partial v}{\partial y}+\frac{1}{2}\left(\frac{\partial w}{\partial y}\right)^2,\ \gamma_{xy}=\frac{\partial u}{\partial y}+\frac{\partial v}{\partial x}+\frac{\partial w}{\partial x}\frac{\partial w}{\partial y},\\ \chi_x=-\frac{\partial^2 w}{\partial x^2},\ \chi_y=-\frac{\partial^2 w}{\partial y^2},\ \chi_{xy}=-2\frac{\partial^2 w}{\partial x\partial y},\end{gathered}\tag{3}$$

Substituting (1) and (2) into the equations of motion gives the system of nonlinear partial integro-differential equations:

$$\begin{gathered}\frac{\partial N_x}{\partial x}+\frac{\partial N_{xy}}{\partial y}=\rho\frac{\partial^2 u}{\partial t^2},\ \frac{\partial N_{xy}}{\partial x}+\frac{\partial N_y}{\partial y}=\rho\frac{\partial^2 v}{\partial t^2},\\ \frac{\partial^2 M_x}{\partial x^2}+\frac{\partial^2 M_y}{\partial y^2}+2\frac{\partial^2 M_{xy}}{\partial x\partial y}+\frac{\partial}{\partial x}\left(N_x\frac{\partial w}{\partial x}+N_{xy}\frac{\partial w}{\partial y}\right)+\\ +\frac{\partial}{\partial y}\left(N_{xy}\frac{\partial w}{\partial x}+N_y\frac{\partial w}{\partial y}\right)+q=\rho\frac{\partial^2 w}{\partial t^2}\end{gathered}\tag{4}$$

If the dynamic process is considered without the propagation of elastic waves, then it becomes possible to discard the inertial terms in the first two equations of the system (3). In this case, the solution of the resulting system has the form described in the articles [22, 23]:

$$\begin{gathered}w\left(x,y,t\right)=\sum_{m=1}^{M}\sum_{n=1}^{N}\left(\gamma_m\cos\frac{\lambda_m x}{a}-\gamma_m\cosh\frac{\lambda_m x}{a}+\sin\frac{\lambda_m x}{a}-\sinh\frac{\lambda_m x}{a}\right)*\\ *\left(\gamma_n\cos\frac{\lambda_n y}{b}-\gamma_n\cosh\frac{\lambda_n y}{b}+\sin\frac{\lambda_n y}{b}-\sinh\frac{\lambda_n y}{b}\right)w_{mn}\left(t\right),\end{gathered}\tag{5}$$

where $w_{mn}(t)$, m, $n=1,2,3,\ldots$ are the unknown functions of time; λ_m and λ_n are the roots of the frequency equation:

$$\cos\lambda_m \cosh\lambda_m = 1$$

and

$$\gamma_m = \frac{\cos\lambda_m - \cosh\lambda_m}{\sin\lambda_m + \sinh\lambda_m}.$$

A system of nonlinear ordinary integro-differential equations is obtained by substituting the approximating function (4) into the resulting system of equations and performing the Bubnov–Galerkin method procedure. Further, this system is integrated using the numerical method [8] based on quadrature formulas. A feature of this numerical method in solving systems of nonlinear integro-differential equations is the preliminary transformation of a singular kernel into a regular one.

3. Results and Discussion

To evaluate the accuracy of the chosen method, we solve a system of nonlinear integro-differential equations of the following form:

$$\begin{gathered}
\ddot{u}+\lambda_1^2 u = p_x + \lambda_2\int_0^t R_1(t-\tau)u(\tau)d\tau + \lambda_3\int_0^t R_2(t-\tau)v(\tau)d\tau + \\
+\lambda_4\int_0^t R_3(t-\tau)w(\tau)d\tau + \lambda_5\int_0^t R_4(t-\tau)w^2(\tau)d\tau, \\
\ddot{v}+\varphi_1^2 v = p_y + \varphi_2\int_0^t R_1(t-\tau)u(\tau)d\tau + \varphi_3\int_0^t R_2(t-\tau)v(\tau)d\tau + \\
+\varphi_4\int_0^t R_3(t-\tau)w(\tau)d\tau + \varphi_5\int_0^t R_4(t-\tau)w^2(\tau)d\tau, \\
\ddot{w}+\omega_1^2 w = q + \omega_2\int_0^t R_1(t-\tau)u(\tau)d\tau + \omega_3\int_0^t R_2(t-\tau)v(\tau)d\tau + \\
+\omega_4\int_0^t R_3(t-\tau)w(\tau)d\tau + \omega_5 w(t)\int_0^t R_1(t-\tau)u(\tau)d\tau + \\
+\omega_6 w(t)\int_0^t R_2(t-\tau)v(\tau)d\tau + \omega_7\int_0^t R_4(t-\tau)w^2(\tau)d\tau
\end{gathered} \tag{6}$$

with initial conditions $u(0)=1$, $\dot{u}(0)=-\beta_1$, $v(0)=1$, $\dot{v}(0)=-\beta_2$, $w(0)=1$, $\dot{w}(0)=-\beta_3$, where

$$R_1(t)=A_1 e^{-\beta_1 t}t^{\alpha_1-1}, \quad R_2(t)=A_2 e^{-\beta_2 t}t^{\alpha_2-1}, \quad R_3(t)=A_3 e^{-\beta_3 t}t^{\alpha_3-1},$$
$$R_4(t)=A_4 e^{-\beta_4 t}t^{\alpha_4-1}, \quad 0<\alpha_1,\ \alpha_2,\ \alpha_3,\ \alpha_4<1;$$

$$p_x=\left(\beta_1^2+\lambda_1^2-\frac{\lambda_2 A_1}{\alpha_1}t^{\alpha_1}\right)e^{-\beta_1 t}-\frac{\lambda_3 A_2}{\alpha_2}e^{-\beta_2 t}t^{\alpha_2}-$$
$$-\frac{\lambda_4 A_3}{\alpha_3}e^{-\beta_3 t}t^{\alpha_3}-\frac{\lambda_5 A_4}{\alpha_4}e^{-\beta_4 t}t^{\alpha_4};$$

$$p_y = \left(\beta_2^2 + \varphi_1^2 - \frac{\varphi_3 A_2}{\alpha_2} t^{\alpha_2} \right) e^{-\beta_2 t} - \frac{\varphi_2 A_1}{\alpha_1} e^{-\beta_1 t} t^{\alpha_1} - \\ - \frac{\varphi_4 A_3}{\alpha_3} e^{-\beta_3 t} t^{\alpha_3} - \frac{\varphi_5 A_4}{\alpha_4} e^{-\beta_4 t} t^{\alpha_4};$$

$$q = \left(\beta_3^2 + \omega_1^2 - \frac{\omega_4 A_3}{\alpha_3} t^{\alpha_3} \right) e^{-\beta_3 t} - \frac{\omega_2 A_1}{\alpha_1} e^{-\beta_1 t} t^{\alpha_1} - \frac{\omega_3 A_2}{\alpha_2} e^{-\beta_2 t} t^{\alpha_2} - \\ - \frac{\omega_5 A_1}{\alpha_1} e^{-(\beta_1+\beta_3)t} t^{\alpha_1} - \frac{\omega_6 A_2}{\alpha_2} e^{-(\beta_2+\beta_3)t} t^{\alpha_2} - \frac{\omega_7 A_4}{\alpha_4} e^{-2\beta_3 t} t^{\alpha_4}.$$

The system of equations (6) has an exact solution: $u = e^{-\beta_1 t}$, $v = e^{-\beta_2 t}$, $w = e^{-\beta_3 t}$, satisfying the initial conditions. Integrating the system of equations (6) twice and taking into account the initial conditions, the approximate values $u_n = u_n(t)$, $v_n = v_n(t)$, $w_n = w_n(t)$ at the nodes $t_n = (n-1)\Delta t$, $n = 1, 2, 3, \ldots$ are found from the relations:

$$u_n = 1 - \beta_1 t_n - e^{-\beta_1 t_n} + \sum_{i=0}^{n-1} B_i (t_n - t_i) \left[p_x(t_i) - \lambda_1^2 u_i + \sum_{k=0}^{i} \left(\frac{\lambda_2 A_1}{\alpha_1} C_{1k} e^{-\beta_1 t_k} u_{i-k} + \right. \right. \\ \left. \left. + \frac{\lambda_3 A_2}{\alpha_2} C_{2k} e^{-\beta_2 t_k} v_{i-k} + \frac{\lambda_4 A_3}{\alpha_3} C_{3k} e^{-\beta_3 t_k} w_{i-k} + \frac{\lambda_5 A_4}{\alpha_4} C_{4k} e^{-2\beta_3 t_k} w_{i-k}^2 \right) \right],$$

$$u_n = 1 - \beta_2 t_n - e^{-\beta_2 t_n} + \sum_{i=0}^{n-1} B_i (t_n - t_i) \left[p_y(t_i) - \varphi_1^2 v_i + \sum_{k=0}^{i} \left(\frac{\varphi_2 A_1}{\alpha_1} C_{1k} e^{-\beta_1 t_k} u_{i-k} + \right. \right. \\ \left. \left. + \frac{\varphi_3 A_2}{\alpha_2} C_{2k} e^{-\beta_2 t_k} v_{i-k} + \frac{\varphi_4 A_3}{\alpha_3} C_{3k} e^{-\beta_3 t_k} w_{i-k} + \frac{\varphi_5 A_4}{\alpha_4} C_{4k} e^{-2\beta_3 t_k} w_{i-k}^2 \right) \right], \quad (7)$$

$$w_n = 1 - \beta_3 t_n - e^{-\beta_3 t_n} + \sum_{i=0}^{n-1} B_i (t_n - t_i) \left[q(t_i) - \omega_1^2 w_i + \sum_{k=0}^{i} \left(\frac{\omega_2 A_1}{\alpha_1} C_{1k} e^{-\beta_1 t_k} u_{i-k} + \right. \right. \\ + \frac{\omega_3 A_2}{\alpha_2} C_{2k} e^{-\beta_2 t_k} v_{i-k} + \frac{\omega_4 A_3}{\alpha_3} C_{3k} e^{-\beta_3 t_k} w_{i-k} + \frac{\omega_5 A_1}{\alpha_1} w_i C_{1k} e^{-\beta_2 t_k} u_{i-k} + \\ \left. \left. + \frac{\omega_6 A_2}{\alpha_2} w_i C_{2k} e^{-\beta_2 t_k} v_{i-k} + \frac{\omega_7 A_4}{\alpha_4} C_{4k} e^{-2\beta_3 t_k} w_{i-k}^2 \right) \right],$$

where $B_i, C_{1k}, C_{2k}, C_{3k}, C_{4k}$ are the coefficients of the quadrature formula;

$$B_0 = h/2,\ B_i = h,\ i = 1, \ldots, n-1;$$

$$C_{l0} = h^{\alpha_l}/2,\ C_{li} = h^{\alpha_l} \left[i^{\alpha_l} - (i-1)^{\alpha_l} \right] \Big/ 2,\ C_{lk} = h^{\alpha_l} \left[\left((k+1) \right)^{\alpha_l} - (k-1)^{\alpha_l} \right] \Big/ 2,$$

$$k = 1, \ldots, n-1,\ l = 1, 2, 3, 4.$$

Table 1 shows the calculation results performed according to (7) in the range from 0 to 0.1 with a step of Δt = 0.0001. The following initial data were used:

$$\lambda_1 = 1.1;\ \lambda_2 = 1.2;\ \lambda_3 = 1.3;\ \lambda_4 = 1.4;\ \lambda_5 = 1.5;$$
$$\varphi_1 = 1.2;\ \varphi_2 = 1.3;\ \varphi_3 = 1.4;\ \varphi_4 = 1.5;\ \varphi_5 = 1.6;$$
$$\omega_1 = 1.3;\ \omega_2 = 1.4;\ \omega_3 = 1.5;\ \omega_4 = 1.6;\ \omega_5 = 1.7;\ \omega_6 = 1.8;\ \omega_7 = 1.9;$$
$$A_1 = 0.01;\ A_2 = 0.02;\ A_3 = 0.03;\ A_4 = 0.04;$$
$$\beta_1 = 0.25;\ \beta_2 = 0.26;\ \beta_3 = 0.27;$$
$$\alpha_1 = 0.05;\ \alpha_2 = 0.06;\ \alpha_3 = 0.07;\ \alpha_4 = 0.08$$

Table 1 also shows that the error of the described method coincides with the error of the quadrature formulas used, and the error is in the same order of smallness relative to the interpolation step.

Table 1. Comparison of approximate and exact solutions.

t	Solution		$\Delta, \%$
	Exact	*Approximate*	
0.0	1.000000000	1.000000000	-
0.01	0.997303642	0.998929533	0.296
0.02	0.994614554	0.997560123	0.397
0.03	0.991932717	0.995866611	0.462
0.04	0.989258111	0.993831608	0.491
0.05	0.986590716	0.991439562	0.482
0.06	0.983930514	0.988675329	0.433
0.07	0.981277485	0.985522169	0.340
0.08	0.978631609	0.981957961	0.200
0.09	0.975992868	0.977947442	0.004
0.10	0.973361242	0.973403577	0.004

In calculations, KAST-V plastic with the following physical and geometric parameters was chosen as the plate material: E_1 = 25.5 GPa, E_2 = 14.91 GPa, G_{12} = 4.41 GPa, μ_{12} = 0.2, ρ = 1900 kg/m^3, $a = b$ = 0.5 m, h = 0.5 sm, θ = 45°, P_0 = 5 MPa/s. The simplest and, at the same time, quite common weakly-singular Koltunov–Rzhanitsyn kernel [24] of the form $\Gamma(t) = Ae^{-\beta t}t^{\alpha-1}\ (0 < \alpha < 1)$ is used as the relaxation kernel where A, α, β are the rheological viscosity parameters determined from the experiments [25].

The graphs below correspond to the results obtained for the midpoint of a rigidly pinched plate under the action of a dynamic load that caused the shift. On the presented graphs, m (meter) is taken as the dimension of the deflection, and *s* (second) is taken as the time.

To ensure the necessary accuracy of the results obtained, the convergence of the Bubnov–Galerkin method was investigated (Fig. 2). The results given below were obtained based on monomial and polynomial approximations. It can be seen from the figure that when calculating the deflection, it is sufficient in (4) to hold the first four harmonics $(M = N = 2)$. The further increase in the number of members does not significantly impact the dynamic process.

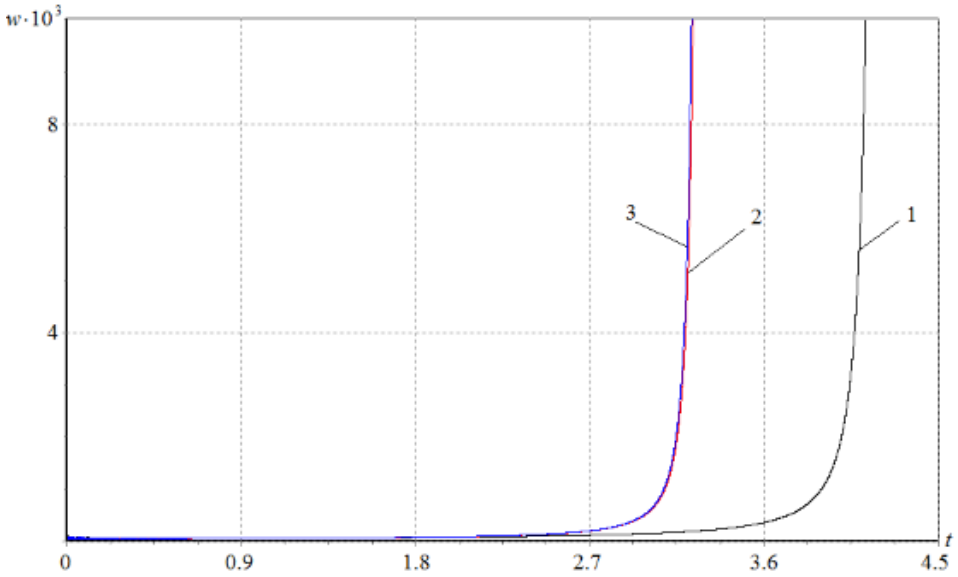

Figure 2. Convergence of the Bubnov–Galerkin method (1 – $M = N = 1$; 2 – $M = N = 2$; 3 – $M = N = 3$).

Fig. 3 illustrate the shape of a deformable rigidly pinched plate under the influence of shear forces. Note that areas with both positive and negative deflections appear on the plate under such loads. It should be noted here that the contact lines of these regions, otherwise called nodal lines or zero deviation lines, do not occur under uniform compressive loads of anisotropic plates. Similar results for elastic static problems were obtained in [22, 23].

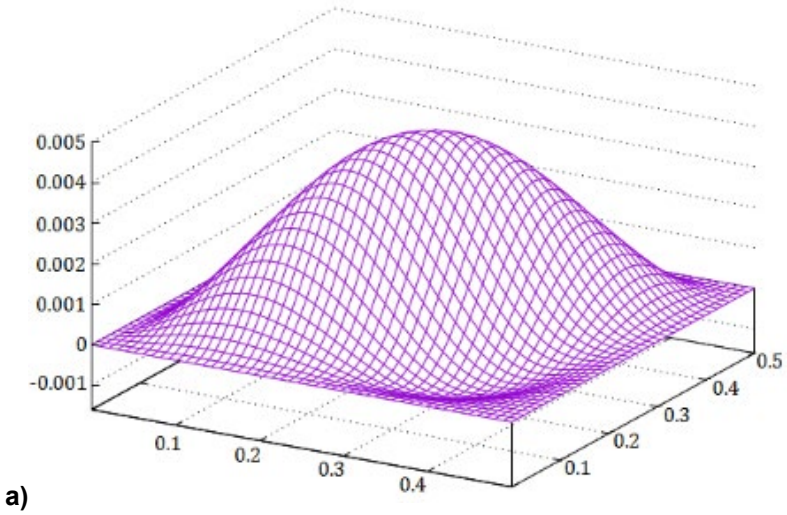

a)

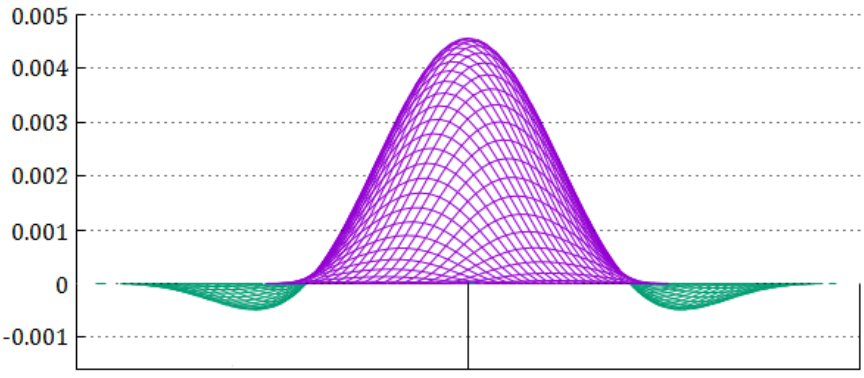

b)

Figure 3. The curved shape of the deformable plate.

The influence of geometric parameters of a rectangular plate on the change of regions with positive and negative deflections is studied (Fig. 4). It is shown that as one of the sides of the plate lengthens, the

area of the region with negative deflections increases. Here λ is the ratio of the sides of the plate. Thus, if λ = 1, then the plate has a square shape.

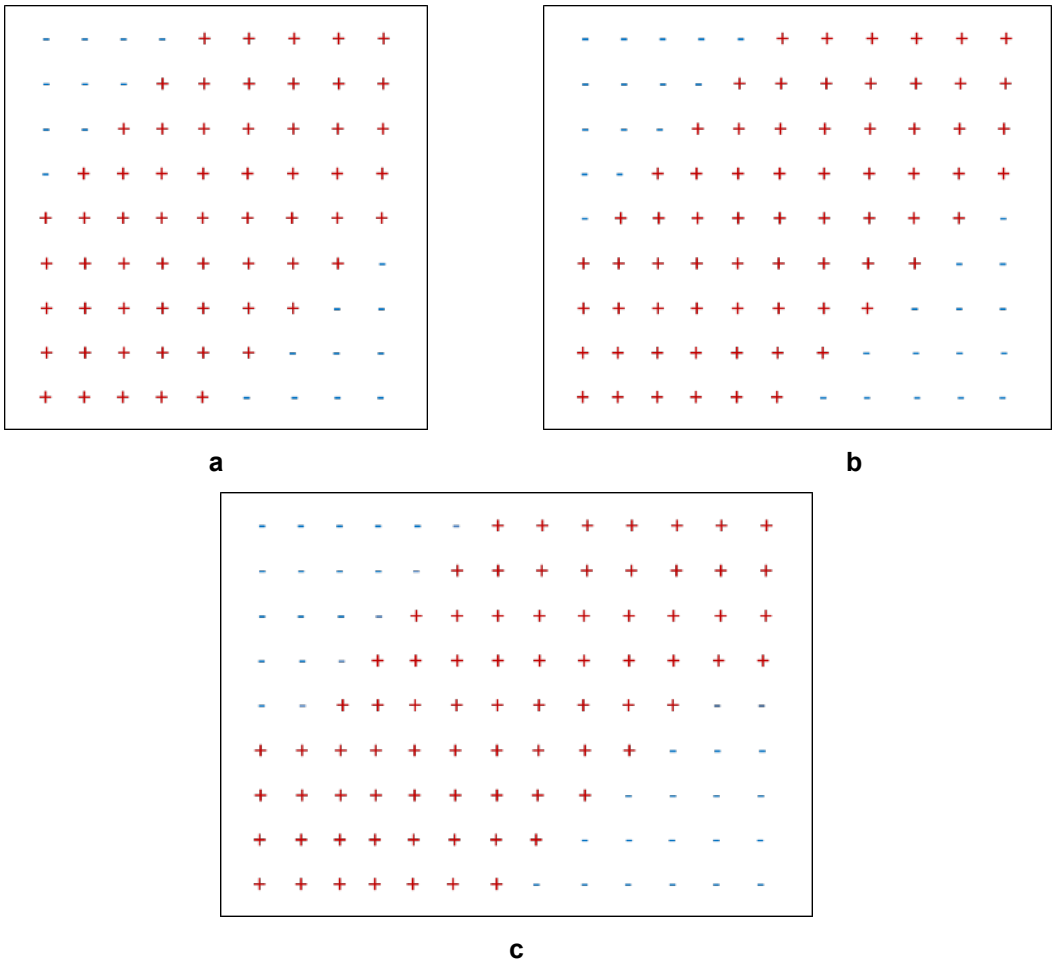

Figure 4. Changing the areas of the plate with positive and negative deflections depending on the change in the surface area of the plate: 1 – λ = 1; 2 – λ = 1.2; 3 – λ = 1.4.

In solving problems about the stability of plates under the influence of compressive dynamic loads, as a criterion determining the critical time and critical load, it is conditionally assumed in [26] that the deflection boom should not exceed an amount equal to the thickness of the plate. With such plate deformations, there are no areas with negative deflections.

In our study, we depart from this convention by considering the presence of areas with both positive and negative deflections in the deformable plate. In our calculations, we define the critical dynamic load as the moment when the difference between the deflection values at the highest and lowest points of the plate (referred to as critical points) equals the plate's thickness. It is worth noting that, unlike the uppermost point of the plate (which remains fixed at the intersection of the diagonals, i.e., the midpoint), the location of the lowest point varies with changes in the physical and geometric parameters of the plate.

Fig. 5 and 6 graphically depict the influence of the material's viscoelastic properties on the behavior of the reinforced plate. In these figures, curves 1 and 2 represent results for the viscoelastic problem while curves 3 and 4 pertain to the elastic scenario $\left(A=0\right)$. Notably, accounting for the viscoelastic properties of the construction material leads to a reduction in the critical time. The disparity in critical time values between elastic and viscoelastic plates, contingent on alterations in the plate's geometric and physical parameters, can exceed 15 %. Furthermore, we observe that a reinforced plate made of EDF with A = 0.0067 is more resistant to shear forces compared to a reinforced plate made of KAST-V with A = 0.0208. This distinction arises from the fact that the latter exhibits more pronounced viscous properties than the former.

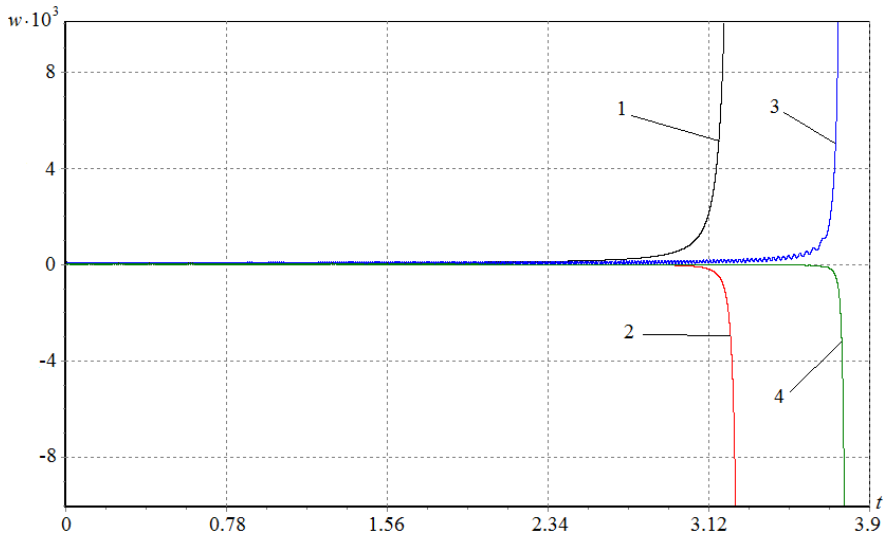

Figure 5. Changing the deflections of the plate from KAST-V at critical points.

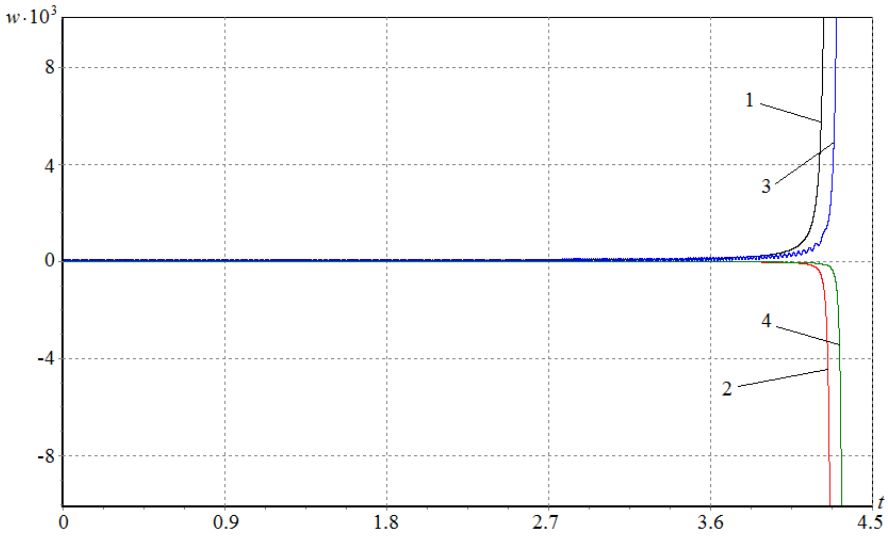

Figure 6. Changing the deflections of the EDF plate at critical points.

An increase in stiffness due to an increase in the thickness of the plate leads to a proportional increase in the critical time value (Fig. 7).

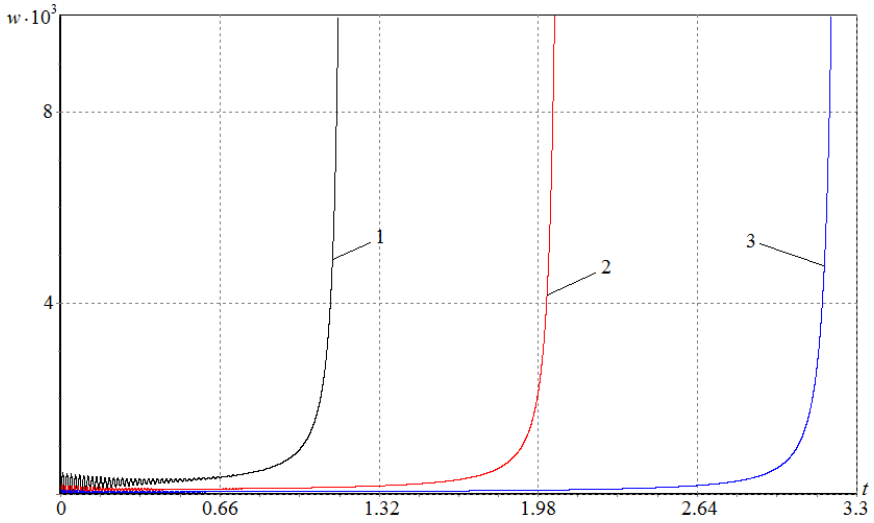

Figure 7. The dependence of the deflection of the reinforced plate on time at different values of its thickness: 1 – h = 0.3 cm; 2 – h = 0.4 cm; 3 – h = 0.5 cm.

Fig. 8 shows similar results for the geometric parameter λ = 1; 1.2; 1.4. As can be seen from the graph, an increase in one of the sides of the plate leads to a shift of the deflection curve to the left (i.e., to a decrease in the critical time).

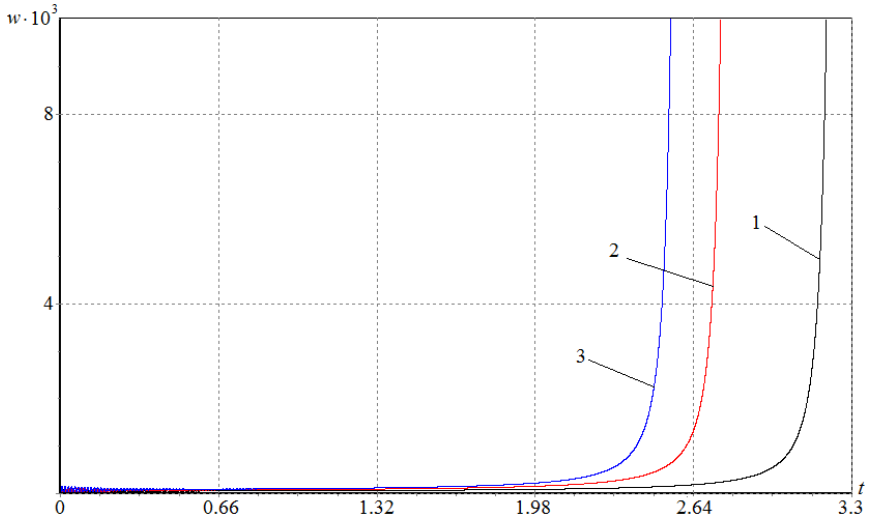

Figure 8. Dependence of the deflection of the reinforced plate on time at different parameter values $\lambda(\lambda = a/b)$: 1 – $\lambda = 1$; 2 – $\lambda = 1.2$; 3 – $\lambda = 1.4$.

In Fig. 9, various curves represent cases involving changes in the deflection of the median point of the reinforced rectangular plate at different loading speeds. As expected, higher loading speeds lead to an earlier increase in deflections. These results are similar to the results obtained in the study of the stability of a simply supported plate under the influence of external compressive loads, given in [10].

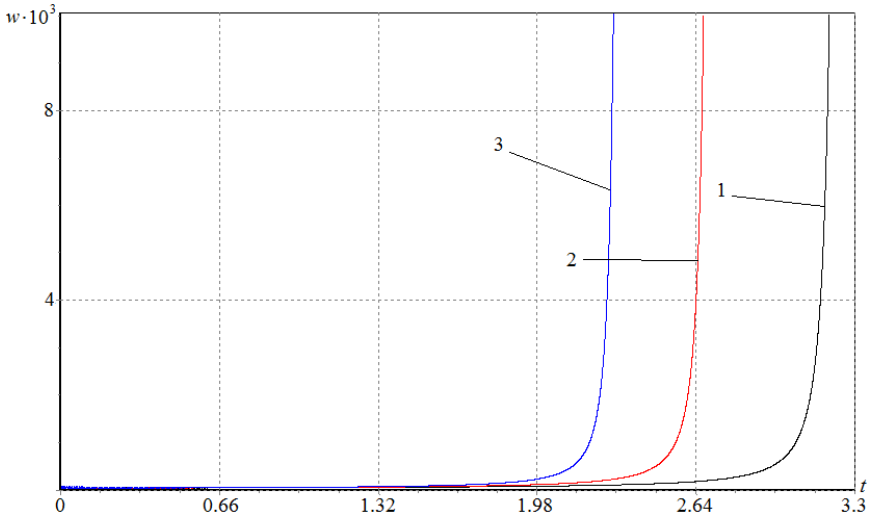

Figure 9. Dependence of the deflection of the reinforced plate on time at different values of loading speeds: 1 – P_0 = 5 MPa/s; 2 – P_0 = 6 MPa/s; 3 – P_0 = 7 MPa/s.

The presented numerical results in Table 2 offer critical time values for an anisotropic reinforced plate constructed from KAST-V material under the influence of rapidly increasing shear loads. These results have been obtained by considering a wide range of variations in the plate's geometric and physical parameters. It is important to note that the values in the table represent the outcomes for both elastic and viscoelastic problems.

As previously mentioned, accounting for the viscoelastic properties of the construction material significantly impacts the numerical results. This effect becomes especially prominent if an anisotropic plate is subjected to an external static load q in addition to shear loads. It is worth highlighting that for large values of q, the stability of the plate is compromised even at relatively low loading speeds.

Layered composites consisting of alternating reinforcing layers, each with different mechanical properties, have found successful applications in various industries. They have the potential to significantly reduce the weight of structures, increase engine efficiency, and facilitate the creation of innovative, highly efficient, and reliable structures. In light of these achievements, the influence of the number of layers and

the orientation of reinforced fibers inside these layers on the dynamic process under consideration has been studied.

This investigation reveals that two-layer plates exhibit greater shear load resistance than single-layer counterparts. For instance, in a two-layer viscoelastic plate with fibers oriented in directions of 45° and –45°, the critical time is more than 1.2 times longer than that of a single-layer plate with fibers oriented in the direction of 45°. However, it is worth noting that further increasing the number of layers may not always be justifiable. In the case of three-layer viscoelastic plates constructed from CAST-V material with fibers oriented in the direction of 45°/–45°/45°, they are less stable than double-layer plates but more stable than single-layer ones while maintaining equal thicknesses across all three structures.

Table 2. Critical time values at different values of geometric and physical parameters of an anisotropic reinforced plate made of KAST-V.

№	Geometric parameters			Physical parameters		Number of layers	Fiber orientations	Critical time values		
	a, m	b, m	h, sm	q, Pa	P_0, MPa/s			Elastic problem	Viscoelastic problem	Difference (in %)
1	0.5	0.5	0.5	100	5	1	45°	3.7325	3.1629	15.3
2	0.6	0.5	0.5	100	5	1	45°	3.2155	2.7211	15.4
3	0.7	0.5	0.5	100	5	1	45°	2.9677	2.5129	15.3
4	0.5	0.5	0.4	100	5	1	45°	2.3838	2.0194	15.3
5	0.5	0.5	0.3	100	5	1	45°	1.3292	1.1240	15.4
6	0.5	0.5	0.5	200	5	1	45°	3.7136	3.1246	15.9
7	0.5	0.5	0.5	300	5	1	45°	3.7009	3.0946	16.4
8	0.5	0.5	0.5	100	6	1	45°	3.1141	2.6452	15.1
9	0.5	0.5	0.5	100	7	1	45°	2.6711	2.2743	14.9
10	0.5	0.5	0.5	100	5	1	0°	4.2618	3.9568	7.2
11	0.5	0.5	0.5	100	5	1	15°	3.9175	3.4630	11.6
12	0.5	0.5	0.5	100	5	1	30°	3.7667	3.2287	14.3
13	0.5	0.5	0.5	100	5	2	0°/90°	4.2861	3.9712	7.3
14	0.5	0.5	0.5	100	5	2	15°/–15°	4.3527	3.8456	11.7
15	0.5	0.5	0.5	100	5	2	30°/–30°	4.5252	3.8704	14.5
16	0.5	0.5	0.5	100	5	2	45°/–45°	4.6053	3.8919	15.5
17	0.5	0.5	0.5	100	5	3	45°/–45°/45°	3.7993	3.2184	15.3

4. Conclusions

The investigation of the dynamic stability of viscoelastic anisotropic reinforced plates exposed to uniformly distributed shear forces along their edges reveals several significant findings:

1. The importance of accounting for the viscoelastic properties of the construction material is evident. Results highlight that the difference in the critical time between solving elastic and viscoelastic problems for plates constructed from KAST-V, contingent on physical and geometric parameters, can exceed 15 %.
2. In layered structures, the critical time values notably depend on the fibers' orientation in each layer. Among the examined cases, the two-layer plate with fibers oriented in directions 0° and 90° demonstrated the highest resistance to shear loads.
3. Changes in the physical and geometric parameters of the plate substantially affect critical time values. Considering the viscoelastic properties of the structural material demonstrates the change in critical time clearly. The results and conclusions drawn from this study enable accurate predictions of the dynamic behavior of reinforced plates made from composite materials.

References

1. Kalusuraman, G., Kumaran, S.T., Balamurugan, K., Sivashanmugam, N., Sivaprakasam, P., Kurniawan, R., Ezhilmaran, V. Vibration Studies on Fiber Reinforced Composites – a Review. Journal of Natural Fibers. 2023. 20(1). Article no. 2157361. DOI: 10.1080/15440478.2022.2157361
2. Sun, C.T., Chattopadhyay, S. Dynamic response of anisotropic laminated plates under initial stress to impact of a mass. Journal of Applied Mechanics. 1975. 42(3). Pp. 693–698. DOI: 10.1115/1.3423664
3. Amuthakkannan, P., Manikandan, V. Free vibration and dynamic mechanical properties of basalt fiber reinforced polymer composites. Indian Journal of Engineering and Materials Sciences. 2018. 25(3). Pp. 265–270.

4. Assarar, M., Zouari, W., Sabhi, H., Ayad, R., Berthelot, J.M. Evaluation of the damping of hybrid carbon-flax reinforced composites. Composite Structures. 2015. 132. Pp. 148–154. DOI: 10.1016/j.compstruct.2015.05.016
5. Biswas, D., Ray, C. Comparative perspective of various shear deformation theories with experimental verification for modal analysis of hybrid laminates. Journal of Vibration and Control. 2017. 23(8). Pp. 1321–1333. DOI: 10.1177/1077546315592766
6. Gopalan, V., Vardhan, M.S., Thakur, V., Krishnamoorthy, A., Pragasam, V., Degalahal, M.R., Velu, P.S., Raja Annamalai, A., Jen, C.-P. Studies on Numerical Buckling Analysis of Cellulose Microfibrils Reinforced Polymer Composites. Materials. 2023. 16(3). Article no. 894. DOI: 10.3390/ma16030894
7. Niyogi, S.B., Wankhade, R.L., Gajbhiye, P.D. Buckling analysis of laminated composites considering the effect of orthotropic material. Journal of Physics: Conference Series. 2020. 1706(1). Article no. 12188. DOI: 10.1088/1742-6596/1706/1/012188
8. Badalov, F., Eshmatov, Kh., Yusupov, M. On certain methods of solving systems of integrodifferential equations encountered in viscoelasticity problems. Journal of Applied Mathematics and Mechanics. 1987. 51(5). Pp. 683–686. DOI: 10.1016/0021-8928(87)90025-6
9. Khodzhaev, D.A., Abdikarimov, R.A., Mirsaidov, M.M. Dynamics of a physically nonlinear viscoelastic cylindrical shell with a concentrated mass. Magazine of Civil Engineering. 2019. 7(91). Pp. 39–48. DOI: 10.18720/MCE.91.4
10. Eshmatov, B.K., Abdikarimov, R.A., Amabili, M., Vatin, N.I. Nonlinear vibrations and dynamic stability of viscoelastic anisotropic fiber reinforced plates. Magazine of Civil Engineering. 2023. 2(118). Article no. 11811. DOI: 10.34910/MCE.118.11
11. Mirsaidov, M., Abdikarimov, R., Khudainazarov, S., Sabirjanov, T. Damping of high-rise structure vibrations with viscoelastic dynamic dampers. E3S Web of Conferences. 2020. 224. Article no. 02020. DOI: 10.1051/e3sconf/202022402020
12. Mohammed, W.H., Shambina, S., Ammash, H.K. Effect of Fibers Orientation on the Nonlinear Dynamic Performance of Laminated Composite Plate under Different Loading In-plane. Civil Engineering Journal. 2022. 8(12). Pp. 2706–2720. DOI: 10.28991/CEJ-2022-08-12-03
13. Kanu, N.J., Lal, A. Nonlinear static and dynamic performance of CNT reinforced and nanoclay modified laminated nanocomposite plate. AIP Advances. 2022. 12(2). Article no. 025102. DOI: 10.1063/5.0074987
14. Parida, S.P., Jena, P.C. Free and forced vibration analysis of flyash/graphene filled laminated composite plates using higher order shear deformation theory. Proceedings of the Institution of Mechanical Engineers, Part C: Journal of Mechanical Engineering Science. 2022. 236(9). Pp. 4648–4659. DOI: 10.1177/09544062211053181
15. Moghaddasi, M., Kiani, Y. Free and forced vibrations of graphene platelets reinforced composite laminated arches subjected to moving load. Meccanica. 2022. 57(5). Pp. 1105–1124. DOI: 10.1007/s11012-022-01476-x
16. Heshmati, A., Jafari-Talookolaei, R.-A., Valvo, P.S., Saadatmorad, M. Free and forced vibration analysis of laminated composite beams with through-the-width delamination by considering the in-plane and out-of-plane deformations. Mechanics of Advanced Materials and Structures. 2023. 1–20. DOI: 10.1080/15376494.2023.2222399
17. Zhu, C., Li, G., Yang, J. Vibration Analysis of Laminated Composite Panels with Various Fiber Angles. Mechanisms and Machine Science. 2023. 125. Pp. 948–956. DOI: 10.1007/978-3-031-15758-5_98
18. Karthikeyan, M., Jenarthanan, M.P., Rakurty, S.V.S.K., Ganesh, K.R.V.S.S. Vibrational and structural analysis of drilled (delaminated) fibre reinforced polymer composite plates. AIP Conference Proceedings. 2023. 2715(1). Article no. 020020. DOI: 10.1063/5.0154528
19. Moorthy, V., Marappan, K. Free and forced vibration analysis of delaminated FRP composite plate with a circular hole. International Journal of Vehicle Noise and Vibration. 2024. 19(3/4). Pp. 203–211. DOI: 10.1504/IJVNV.2023.136068
20. Mirzaei, M., Rabiei, R. On the free and forced vibrations of porous GPL reinforced composite conical panels using a Legendre-Ritz method. Engineering Analysis with Boundary Elements. 2024. 163. Pp. 378–393. DOI: 10.1016/j.enganabound.2024.03.024
21. Jones, R.M. Mechanics of Composite Materials. Second Edition. Boca Raton: CRC Press, 2018. 519 p.
22. Whitney, J.M. Structural Analysis of Laminated Anisotropic Plates. Lancaster, PA: Technomic Pub. Co, 1987. 342 p. DOI:
23. Ashton, J.E., Whitney, J.M. Theory of Laminated Plates. Stamford, CT: Technomic, 1970. 158 p.
24. Koltunov, M.A. Choice of kernels in solving problems involving creep and relaxation. Polymer Mechanics. 1966. 2(4). Pp. 303–311. DOI: 10.1007/BF00860064
25. Tyuneeva, I.M. Relaxation characteristics of glass-reinforced plastics. Polymer Mechanics. 1970. 6(3). Pp. 492–494. DOI: 10.1007/BF00858221
26. Volmir, A.S. The nonlinear dynamics of plates and shells. Dayton, OH: Foreign Technology Division Wright-Patterson Air Force, 1974. 543 p.

Information about the authors:

***Bakhtiyor Eshmatov**,*
ORCID: https://orcid.org/0000-0003-0198-6679
E-mail: ebkh@mail.ru

***Mirziyod Mirsaidov**, Doctor of Technical Sciences*
ORCID: https://orcid.org/0000-0002-8907-7869
E-mail: mirsaidov1948@mail.ru

***Rustamkhan Abdikarimov**, Doctor of Physics and Mathematics*
ORCID: https://orcid.org/0000-0001-8114-1187
E-mail: rabdikarimov@mail.ru

***Nikolai Vatin**, Doctor of Technical Sciences*
ORCID: https://orcid.org/0000-0002-1196-8004
E-mail: vatin@mail.ru

Received 11.04.2024. Approved after reviewing 16.07.2024. Accepted 20.07.2024.